Cyclic Elastoplastic Large Displacement Analysis and Stability Evaluation of Steel Tubular Braces

Iraj H. P. Mamaghani [a*]

a *Department of Civil Engineering, School of Engineering and Mines, University of North Dakota, USA.*

A R T I C L E I N F O

A B S T R A C T

This paper deals with the cyclic elastoplastic large displacement analysis and stability evaluation of steel tubular braces subjected to axial tension and compression. The inelastic cyclic performance of cold-formed steel braces made of circular hollow sections is examined through finite element analysis using the commercial computer program ABAQUS. First some of the most important parameters considered in the practical design and ductility evaluation of steel braces of tubular sections are presented. Then the details of finite element modeling and numerical analysis are described. Later the accuracy of the analytical model employed in the analysis is substantiated by comparing the analytical results with the available test data in the literature. Finally the effects of some important structural and material parameters on cyclic inelastic behavior of steel tubular braces are discussed and evaluated.

1. Introduction

Steel braced frames are one of the most commonly used structural systems because of their structural efficiency in providing significant lateral strength and stiffness. The steel braces

contribute to seismic energy dissipation by deforming inelastically during an earthquake. The use of this type of construction indeed avoids the brittle fractures found in beam-to-column connections in moment-resisting steel frames that occurred in the Northridge earthquake in 1994 and the Kobe earthquake in 1995 (ASCE, 2000; *IGNTSDSS* , 1996). However, careful design of steel braced frames is necessary to avoid possible catastrophic failure by brace rupture in the event of severe seismic loading. The current capacity design procedure adopted in most seismic design steel specifications (AISC, 1997; CAN-CSA S16.1, 1989), for concentrically braced frames requires yielding in the braces as primary members, whereas the secondary members of the frame should remain elastic and hence carry forces induced by the yielding members. The transition from current perspective seismic codes to performance-based design specifications requires accurate predictions of inelastic limit states up to structural collapse.

The cyclic behavior of steel brace members is complex due to the influence of various parameters such as material nonlinearity, structural nonlinearity, boundary condition, and loading history. The material nonlinearity includes structural steel characteristics such as residual stresses, yield plateau, strain hardening and Bauschinger effect. The structural nonlinearity includes parameters such as brace slenderness, cross-section slenderness, width-to-thickness ratio of the cross-section's component elements (or radius-to-thickness ratio of circular hollow sections), and initial out-of-straightness of the brace. This complex behavior results in various physical phenomena, such as yielding in tension, buckling in compression, postbuckling deterioration of compressive load capacity, deterioration of axial stiffness with cycling, and low- cycle fatigue fractures at plastic regions.

Steel braces can be designed to resist only tensile forces, or to resist both tensile and compressive axial forces. Recent earthquakes and experiments have shown that the tension-compression braces provide better performance under cyclic loading (during an earthquake) as compared with the tension-only braces having almost no compressive strength (IGNTSDSS, 1996). Under severe earthquakes, the braces are subjected to cyclic axial forces and they are allowed to undergo compression buckling or tensile yield to dissipate the imposed energy while columns and collector beams respond elastically. Therefore, understanding the behavior of the bracing members under idealized cyclic loading is an important step in the careful design of steel braced frames.

Iraj H.P. Mamaghani

This paper deals with the inelastic cyclic analysis of steel tubular braces. The most important parameters considered in the practical design and ductility evaluation of steel braces of tubular sections are presented. The cyclic performance of steel tubular braces is examined through finite element analysis using the computer program ABAQUS (2005). The accuracy of the analytical model employed in the analysis is substantiated by comparing the analytical results with the available test data in the literature. The effects of some important structural and material parameters on inelastic cyclic behavior of steel braces are discussed and evaluated.

2. Brace Parameters

Energy absorption through hysteretic damping is one of the great interests in seismic design, because it can reduce the amplitude of seismic response, and thereby reduce the ductility demand on the structure. Steel braces are very effective structural members and are widely used as energy dissipaters in skeletal buildings and offshore structures under extreme loading conditions such as severe earthquake and wave motion. They also minimize story drift of high-rise buildings for possible moderate earthquakes during their lifetime.

The most important parameters considered in the practical design and ductility evaluation of steel braces of tubular sections are section slenderness λ_s (Mamaghani, et. al., 1996a, 1996b, 1997; Mamaghani, 2005, 2008) and slenderness ratio of the member λ_c (AISC, 1997, 1999). While the former influences local buckling of the section, the latter controls the overal stability. They are given by:

$$\lambda_s = \frac{1}{\pi}\frac{b}{t}\sqrt{3(1-v^2)\frac{\sigma_y}{E}} \quad \left(for\ box\ sec tion\right) \tag{1}$$

$$\lambda_s = \frac{d}{2t}\sqrt{3(1-v^2)}\frac{\sigma_y}{E} \quad \left(for\ circular\ sec tion\right) \tag{2}$$

$$\lambda_c = \frac{1}{\pi}\frac{KL}{r}\sqrt{\frac{\sigma_y}{E}} \tag{3}$$

*Corresponding author (**Iraj H.P. Mamaghani**). Tel: +1-701-777 3563, Fax: +1-701-777 3782. E-mail address: iraj.mamaghani@engr.und.edu.

where, b = flange width of a box section; t = plate thickness of the cross-section elements; σ_y = measured yield stress; E = Young's modulus; v = Poisson's ratio; d = outer diameter of the circular section; K = effective length factor; L = measured length of the brace; and r = radius of gyration of the cross section. It is worth noting that the section slenderness, λ_s, represents the width-thickness ratio parameter of the flange plate for a box section and the diameter-thickness ratio of a circular hollow section for a given material.

The limiting diameter-thickness ratio specified in AISC (1997) for plastic design of circular hollow sections is $d/t = 0.045E/\sigma_y$. This d/t limit can be converted to a limiting slenderness parameter for a compact element according to Equation 2. The corresponding value of λ_s, considering $v = 0.3$ for structural steels, is:

$$\lambda_s = \frac{0.045E}{2\sigma_y}\sqrt{3(1-0.3^2)}\frac{\sigma_y}{E} = 0.037 \tag{4}$$

This implies that when $\lambda_s \leq 0.037$, no local buckling occurs before the cross-section attains full plastic capacity. The limiting width-thickness ratio specified in AISC (1997) for non-compact circular hollow sections is $d/t = 0.11E/\sigma_y$ which corresponds to $\lambda_s = 0.09$. The ductility behavior of the circular hollow section braces is significantly sensitive to λ_s when it is less than 0.09. The maximum member slenderness limits specified in AISC (1997) for special concentrically braced frames (SCBF) and ordinary concentrically braced frames are $\lambda_c = 1.87$ ($KL/r \leq 1000/\sqrt{\sigma_y}$) and $\lambda_c = 1.35$ ($KL/r \leq 720/\sqrt{\sigma_y}$), respectively. SCBF are expected to withstand significant inelastic deformation when subjected to the force resulting from the motion of the design earthquake. SCBF have increased ductility due to lesser strength degradation when compression braces buckle.

3. Numerical Method

Steel braces are vulnerable to damage caused by local and overall interaction buckling during a major earthquake. A sound understanding of the inelastic behavior of steel braces is important in developing a rational seismic design methodology and ductility evaluation of steel braced frame structures.

Iraj H.P. Mamaghani

An accurate cyclic analysis of braced frames requires precise methods to predict the cyclic inelastic large-deflection response of the braces.   This has been a subject of intensive research and a variety of analytical methods have been developed to simulate the hysteretic behavior of braces over the past few decades. The main research approaches used for the cyclic analysis of braces may be classified as: (1) empirical models, (2) plastic-hinge models, and (3) elastoplastic finite element models (Mamaghani et al., 1996a). The more accurate models were based on the finite element method considering geometric and material nonlinearities. This method is generally applicable to many types of problems, and it requires only the member geometry and material properties (constitutive law) to be defined.

3.1 Finite Element Method

The finite element analysis is carried out by using the commercial computer program ABAQUS. The shell element S4R is used in modeling the brace member (ABAQUS, 2005). The S4R element is a three-dimensional, double-curved, four-node shell element with six degrees of freedom per node that uses bilinear interpolation. Because the S4R element contains only one sample point while five layers are assumed across the thickness, the spread of plasticity is considered through both the thickness and plane of the element. This shell element, which uses reduced integration, is applicable to both thin and thick shells, and can be used for finite strain applications.

In the analysis, both material and geometrical nonlinearities are considered. For large displacement analysis, the elements are formulated in the current configuration, using current nodal positions. Elements therefore distort from their original shapes as the deformation increases. The stiffness matrix of the element is obtained from the variational principle of virtual work. The modified Newton-Raphson iteration technique coupled with the displacement control method is used in the analysis (Zienkiewicz, 1977). The displacement convergence criterion is adopted and the convergence tolerance is taken as 10^{-5}. The details of elastoplastic large-displacement formulation and solution scheme are reported in the work by the author (Mamaghani, 1996).

*Corresponding author (**Iraj H.P. Mamaghani**). Tel: +1-701-777 3563, Fax: +1-701-777 3782. E-mail address: iraj.mamaghani@engr.und.edu.

3.2 Analytical Modeling

A series of numerical studies on the cyclic behavior of steel braces are carried out using the numerical finite element method described in the previous section, and the results are compared with the experiments. The results for three typical examples, S7A, S7B, and S7C (Elchalakani et al., 2003), presented hereafter are intended to verify the accuracy of the numerical method. These specimens are subjected to three loading histories in order to better understand the cyclic behavior of cold-formed circular hollow-section braces. The details of the test can be found in Elchalakani et al. (2003).
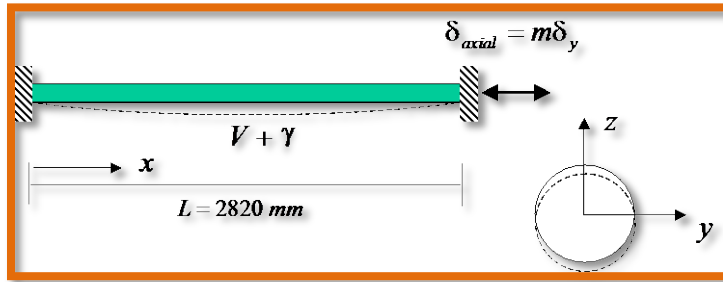

Figure 1: Analyzed circular hollow section steel brace and initial imperfection.

Table 1: Properties of the analyzed braces.

Test Number	Specimen Shape	A_g (mm^2)	L (mm)	λ_s	λ_c	δ_y (mm)	P_y (kN)
S7A	CHS 139.7x3.5	1498	2820	0.06	0.4	5.34	568
S7B	CHS 139.7x3.5	1498	2820	0.06	0.4	5.34	568
S7C	CHS 139.7x3.5	1498	2820	0.06	0.4	5.34	568

The shape and dimensions of the analyzed braces are given in Table 1. For comparison, the selected brace parameters ($\lambda_c = 0.4$ and $\lambda_s = 0.06$) are kept the same. These parameters represent a non-compact member having inelastic behavior. The analyzed fixed-end tubular braces subjected to cyclic concentric axial loading are modeled as shown in the Figure 1.   An initial imperfection of

$$\gamma_x = \gamma_0 \sin\left(\frac{\pi x}{L}\right) \tag{5}$$

is assumed in the analysis, where the initial deflection at midspan of the member γ_0 is taken as the measured value of L/3160 during the test.
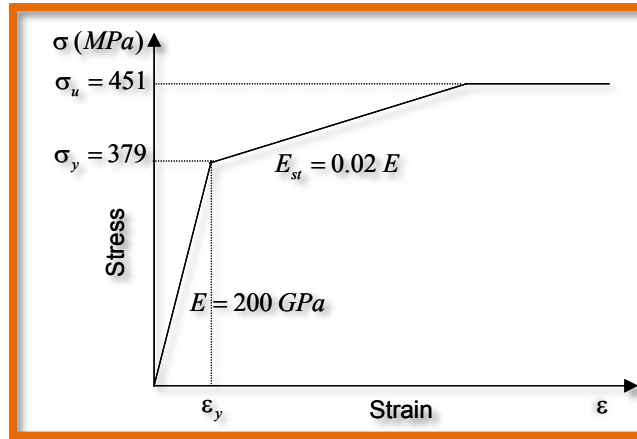
Figure 2: Tri-linear stress-strain model for steel.

3.3 Material Model

The analyzed cold-formed circular hollow sections are AS 1163 grade C350L0 (equivalent to ASTM A500 tubes) with the yield stress of $\sigma_y = 379$ MPa and the ultimate tensile strength of $\sigma_u = 451$ MPa. In the analysis, the material nonlinearity is accounted for by using the kinematic hardening rule. Figure 2 shows the tri-linear stress-strain material model adopted in the analysis. The Young modulus of elasticity of the steel is assumed to be $E = 200$ GPa. The strain hardening modulus is assumed to be 2 percent of the initial Young modulus ($E_{st} = 0.02E$).
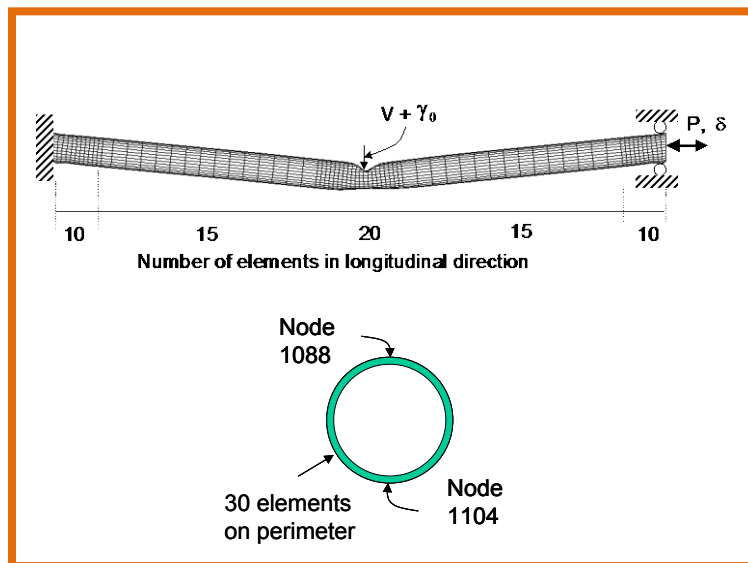

Figure 3: Meshing details and boundary conditions.

*Corresponding author (**Iraj H.P. Mamaghani**). Tel: +1-701-777 3563, Fax: +1-701-777 3782. E-mail address: iraj.mamaghani@engr.und.edu.

3.4 Cyclic Loading History

In the analysis three cyclic loading histories are applied. The first loading history is a large compression-tension monocycle with a maximum normalized displacement amplitude $m = \delta_{max} / \delta_y$, where δ_{max} is the maximum displacement in the compression-half cycle at load reversal and $\delta_y = \varepsilon_y L = P_y L / EA$ is the yield displacement corresponding to the squash load of cross section $P_y = \sigma_y A$ (A = area of the cross-section; σ_y = yield stress; L = the length of the brace). The large amplitude used in the monocycle is applied to examine the inelastic response of the brace when subjected to a very large seismic demand during a possible near-field excitation (Krawinkler et al., 2000). The second loading history is a uniform increase of displacement amplitude up to failure with the maximum normalized displacement amplitudes of m = 1, 2, 3, …, where each amplitude is repeated only once. In the third loading history, a uniform increase of the displacement is used similar to the second loading history except that the oscillations are repeated three times at each amplitude (m = 1, 2, 3, …, etc.).

3.5 Finite Element Meshing and Boundary Conditions

The details of the finite-element meshing pattern adopted in the analysis of hollow circular sections are shown in Figure 3. The brace is subdivided into a total number of 2100 shell elements (70 elements along the brace length and 30 elements in the circumferential direction). A finer mesh pattern is used at the center and the ends of the brace, where large deformation is expected, as shown in Figure 3. In the analysis, the left end of the brace is fully fixed and the right end is modeled as a guided support to apply axial displacement, as shown in Figure 3. The axial load, P, and vertical deflection at midspan, V, are obtained from analysis.

4. Numerical Results

4.1 Example 1

The first example is concerned with the analysis of the brace S7A, which has a nominal length of 2820 mm, a member slenderness parameter of λ_c = 0.4 and a section slenderness of λ_s = 0.06 (Table 1). These parameters represent a non-compact member having inelastic behavior.

This brace is subjected to a large compression-tension monocycle with maximum normalized displacement amplitude of m = 18.24 (the first loading history) to examine the inelastic response of

the brace under a very large seismic demand. This value is larger than the upper limit for $m = 10$, which is likely to occur in a near-source excitation (Krawinkler et al., 2000). In order to check the effects of mesh density and loading increment (loading time steps) on the inealstic cyclic behavior of the brace, three analyses are carried out on this brace. The first analysis, designated as the original analysis, uses the original meshing pattern shown in Figure 3 with a total number of 2100 shell elements. The second analysis, designated as the mesh-increment analysis, uses a finer mesh density at the central segment and at the ends of the brace by doubling the mesh number in these regions with a total number of 3300 shell elements. The third analysis, designated as the step-increment analysis, utilizes the original meshing but doubling the time step by reducing the displacement increment to half of that used in the original analysis. Figures 4a and 4b compare the normalized axial load P / P_y -axial deformation δ / δ_y hysteresis loop obtained from the experiment and analyses. With reference to these figures, the following observations can be made:

1. The initial stiffness and buckling load capacity are slightly lower in the experiment than those predicted by the analyses using various mesh sizes and loading incremens. This may be due to the experimental boundary conditions (unavoidable rotation at the fix-ends) and the assumed initial imperfection in the analysis. In the analysis the cross-section out-of-straightness and residual stress are not accounted for. It is worth noting that the previous research by the author indicates that the initial residual stresses and initial section imperfections significantly decrease the initial stiffness and initial buckling load capacity and have almost no effect on the subsequent cyclic behavior of the member (Mamaghani et al., 1996a, Banno et al., 1998).

2. Under compressive load, the overall buckling was followed by local buckling at the center and brace ends. From Figures 4a and 4b, it can be observed that the overall shape of the predicted hysteresis loop is significantly closer to the experiment.

3. Under tension load, the behavior of the brace is well predicted up to $\delta / \delta_y = 9.3$, where there is a sharp decrease in predicted tensile strength beyond this displacement. The observed discrepancy between experimental and analytical results when the specimen is stretched beyond $\delta / \delta_y = 9.3$ might be due to the formation of a plastic hinge at the member midspan under combined biaxial hoop stress and axial stress. By further stretching the

member, the spread of plasticity fully covered the whole cross section at midspan and extended on both sides of this section, leading to the reduction of load carrying capacity, see Figure 5.
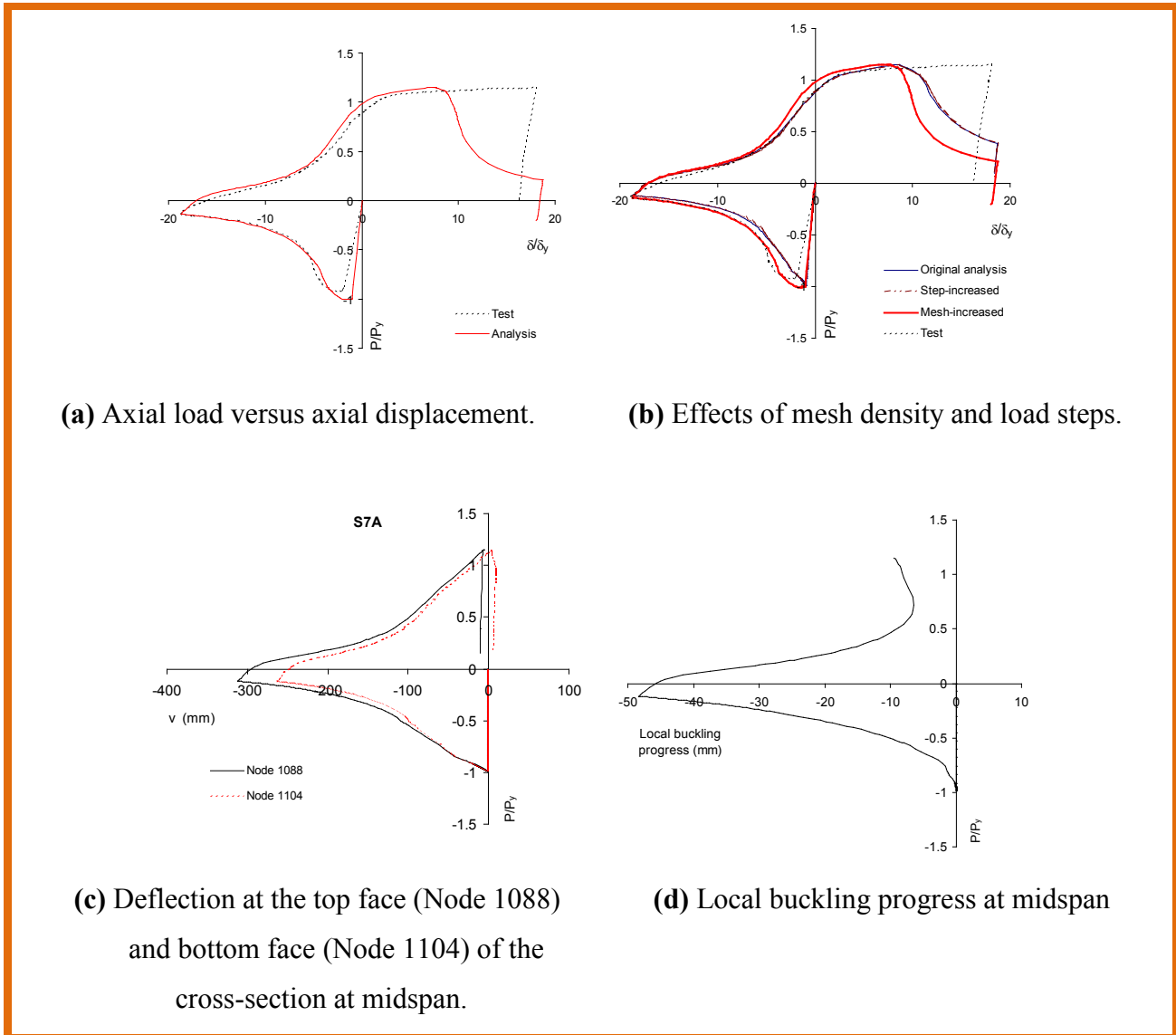

(a) Axial load versus axial displacement.

(b) Effects of mesh density and load steps.

(c) Deflection at the top face (Node 1088) and bottom face (Node 1104) of the cross-section at midspan.

(d) Local buckling progress at midspan

Figure 4: Comparison between experimental and predicted hysteretic loop for brace S7A.

4. The results in Figure 4(b) show that the increase in time step and use of fine mesh do not have significant effects on the overall predicted behavior except for a slight improvement in postbuckling behavior where the predicted results closely fit the test results. Under tensile loading beyond the $\delta / \delta_y = 9.3$, the predicted tensile load capacity drops slightly earlier

for the analysis using fine mesh as compared with the other analyses. This is because the spread of plasticity and formation of the plastic hinge takes place faster for the fine mesh model.

Figure 4(c) shows normalized axial load P/P_y versus vertical deflection V, at the top face (Node 1088) and bottom face (Node 1104) of the cross-section at the midspan of the member (Figure 3), obtained from the analysis. The results in this figure show that the relative vertical deflection at the top and bottom faces of the cross-section at midspan increases as the member undergoes large axial deformation. The difference between the vertical displacements of the top face and bottom face at midspan indicates the progress of local buckling, which is plotted in Figure 4(d). Figure 5 shows the deformation of the specimen at the end of compression load and tension stretching. Under compression load, the overall buckling was followed by local buckling at the center and brace ends. A smooth kink formed at midspan of the brace under compression load. A semi-elephant-foot (an outward folding mechanism) was formed at the fixed ends of the brace, as shown in Figure 5. During the tensile stretching, the brace suffered excessive stretching at the midspan because of the development of a plastic hinge caused by a very large accumulation in local deformation. This represents a tear-through-failure mode, as the specimen exhibited during the test (Elchalakani et al., 2003). These observed behaviors under compression and tension loads are reflected in the normalized load-displacement hysteretic loop shown in Figure 4.

4.2 Example 2

The second example is concerned with the analysis of the brace S7B, which has a nominal length of 2820 mm, a member slenderness of $\lambda_c = 0.4$ and a section slenderness of $\lambda_s = 0.06$ (Table 1). This brace is subjected to a uniform increase of displacement amplitude up to failure with the maximum normalized displacement amplitudes of $m = 1, 2, 3, \ldots$, where each amplitude is repeated only once (the second loading history). The original meshing pattern shown in Figure 3, with a total number of 2100 shell elements, is utilized in the analysis.
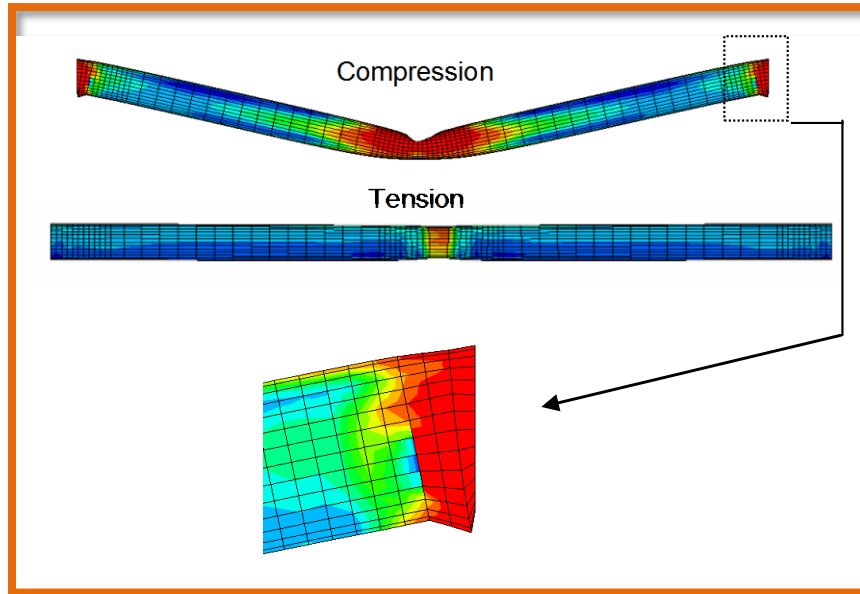
Figure 5: Deformed configuration of brace S7A at the final stage of compression and tension cyclic loading.

Figure 6(a) compares the normalized axial load P/P_y -axial deformation δ/δ_y hysteresis loops obtained from the experiment and analysis. Figure 6(b) shows the normalized axial load P/P_y versus vertical deflection V, at the midspan of the member (Figure 3), obtained from the analysis. Comparison between hysteresis loops in Figure 6(a) shows that there is a relatively good agreement between analytical results and experiments. An observed small discrepancy between experimental and analytical hysteresis loops is that the predicted cyclic load capacities in compression direction of loading are slightly higher than those of the experiment. The possible reasons are: (a) the tri-linear kinematic hardening rule adopted in the analysis does not accurately consider the reduction of the elastic range due to plastic deformation (Bauschinger effect). In this model the size of the elastic range is taken to be constant which does not represent the actual behavior of structural steel (Mamaghani et al. 1995; Shen et al., 1995). More accurate results can be obtained from analysis using a cyclic constitutive law representing the more realistic behavior of the material; (b) the brace fixed-end boundary conditions may have shown some degree of flexibility during the tests, which is not considered in the analysis; and (c) in the analysis the cross-section's out of straighness and residual stresses, which affect the initial buckling load, are not considered.
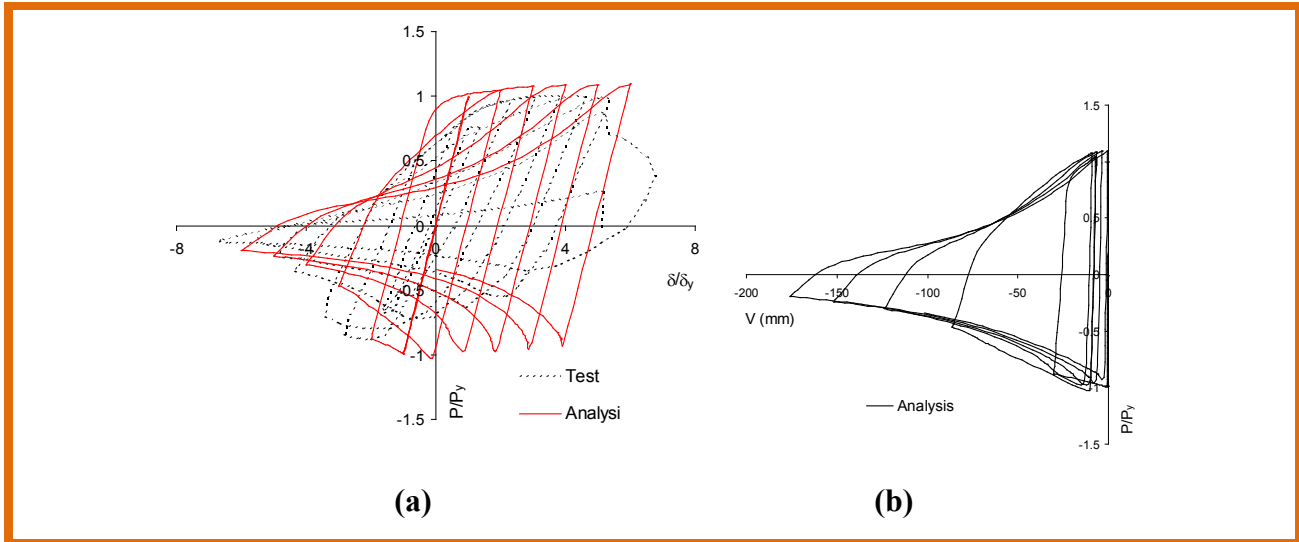
Figure 6: Comparison between experimental and predicted hysteretic loop for brace S7B.

Figure 6(b) shows that there is a residual midspan deflection at the end of tensioning in each cycle. The residual deflection of the brace at the end of the previous tensioning has   a large effect on the buckling capacity and subsequent cyclic behavior. Figure 6(b) shows the progress of residual midspan deflection due to cycling obtained from analysis. In spite of large progress in buckling, the buckling load does not decrease significantly due to cyclic strain hardening.

4.3   Example 3

The third example is concerned with the analysis of the brace S7C, which has a nominal length of 2820 mm, a member slenderness of $\lambda_c = 0.4$ and a section slenderness of $\lambda_s = 0.06$ (Table 1). This brace is subjected to a uniform increase in displacement amplitude up to failure with the maximum normalized displacement amplitudes of $m = 1, 2, 3, \ldots$, where each amplitude is repeated three times (the third loading history). The original meshing pattern as shown in Figure 3, with a total number of 2100 shell elements, is utilized in the analysis.

Figure 7(a) compares the normalized axial load P/P_y -axial deformation δ/δ_y hysteresis loop obtained from experiment and analysis. Figure 7(b) shows the normalized axial load P/P_y versus vertical deflection V, at the midspan of the member (Figure 3), obtained from the analysis. Comparison between hysteresis loops in Figure 7(a) shows there is a relatively good agreement

*Corresponding author (**Iraj H.P. Mamaghani**). Tel: +1-701-777 3563, Fax: +1-701-777 3782. E-mail address: iraj.mamaghani@engr.und.edu.

between analytical results and experiments. These results indicate that the numerical method and finite element modeling employed in the numerical analysis can predict with a reasonable degree of accuracy the experimentally observed cyclic behavior of axially loaded fixed-end steel braces of circular hollow sections.
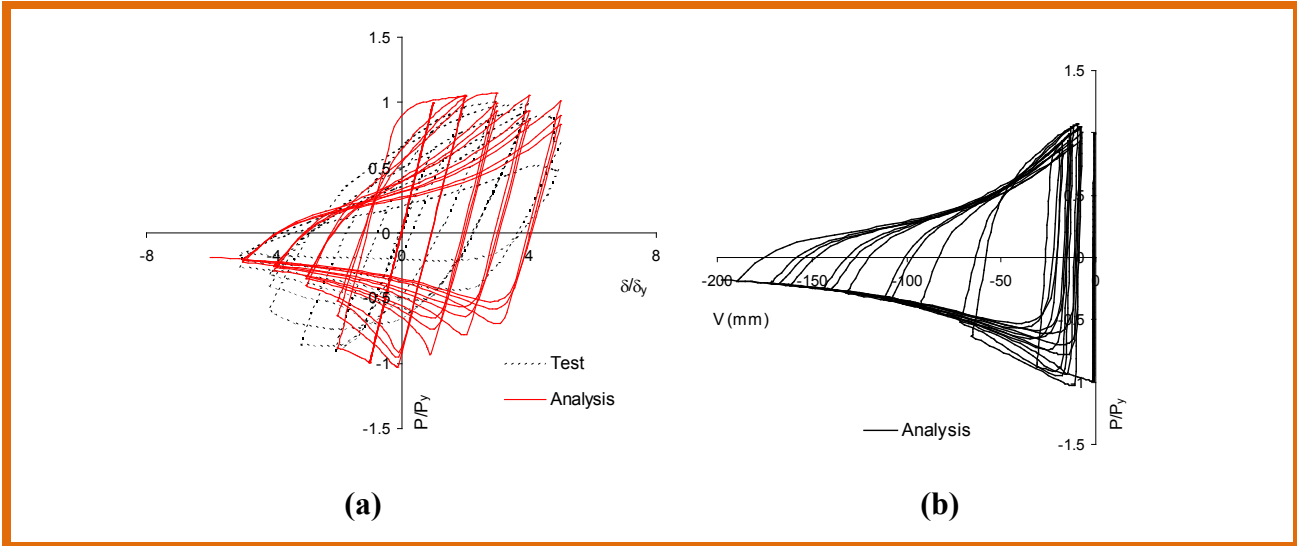

Figure 7: Comparison between experimental and predicted hysteretic loop for brace S7C.

5. Conclusions

This paper dealt with the inelastic cyclic elastoplastic finite-element analysis and stability (strength and ductility) evaluation of steel tubular braces subjected to axial tension and compression. The most important parameters considered in the practical seismic design and ductility evaluation of steel braces of tubular sections, such as brace slenderness, cross-section slenderness, material behavior, and loading history, were presented. The elastoplastic cyclic performance of cold-formed steel braces of circular hollow sections was examined through finite-element analysis using the commercial computer program ABAQUS and employing a tri-linear kinematic strain hardening model to account for material nonlinearity. The details of finite element modeling and numerical analysis were described. The accuracy of the analytical model employed in the analysis was substantiated by comparing the analytical results with the available test data in the literature. The effects of some important structural, material, and loading history parameters on cyclic inelastic behavior of steel braces were discussed and evaluated with reference to the experimental and analytical results. It has been shown that the numerical method and finite element modeling employed in the numerical analysis can predict with a reasonable

degree of accuracy the experimentally observed cyclic behavior of axially loaded fixed-end steel braces of circular hollow sections.

6. References

ABAQUS / Standard User's Manual. (2005). Ver. 6.5, Hibbitt, Karlsson and Sorensen, Inc.

Amrican Institute of Steel Constructions (AISC-LRFD). (1999). Load and resistance factor design specification for structural steel buildings, 3rd Edition, Chicago.

Amrican Institute of Steel Constructions (AISC).   (1997). Seismic provisions for structural steel
buildings, Chicago, Illinois.

ASCE.   (2000). Steel moment frames after Northridge. *J. Struct. Eng.*, 126(1) (special issue).

Banno, S., Mamaghani, I. H.P., Usami, T., and Mizuno, E. (1998). Cyclic elastoplastic large deflection analysis of thin steel plates. *Journal of Engineering Mechanics,* ASCE, USA,Vol. 124, No. 4, pp. 363-370.

Canadian Standards Associations (CAN-CSA S16.1).   (1989). Steel structures for buildings, limit
state design.

Elchalakani, M., Zhao, X. L., Grzebieta, R. (2003). Test of cold-formed circular tubular braces under cyclic axial loading. J. of Struct. Eng., ASCE, 129(4), pp. 507-514.

Interim Guidelines and New Technologies for Seismic Design of Steel Structures (IGNTSDSS).
(1996). In T., Usami (eds), Committee on New Technology for Steel Structures,
Japan Society of Civil Engineers (JSCE), Japan,(in Japanese).

Krawinkler, R., Akshay, G., Medina, R., and Luco, M. (2000). Development of loading histories for testing of steel-to-beam assemblies. Report prepared for SAC Steel Project, Dept. of Civil and Environmental Engineering, Stanford University.

Mamaghani, I.H.P. (2008). Seismic Design and Ductility Evaluation of Thin-Walled Steel Bridge Piers of Box Sections, Transportation Research Record: *Journal of the Transportation Research Board*, Volume 2050, pp. 137-142.

Mamaghani, I.H.P. (2005). Seismic performance evaluation of thin-walled steel tubular columns, *Structural Stability*, Structural Stability Research Council, Montreal, Quebec, Canada, pp.1-10.

Mamaghani, I.H.P. (1996). Cyclic elastoplastic behavior of steel structures: theory and experiments. *Doctoral Dissertation,* Department of Civil Engineering, Nagoya University,

Nagoya, Japan.

Mamaghani, I.H.P., Usami, T., and Mizuno, E. (1996a). Inelastic large deflection analysis of structural steel members under cyclic loading. *Engineering Structures*, UK, Elsevier Science, 18(9), pp. 659-668.

Mamaghani, I.H.P., Usami, T., and Mizuno, E. (1996b). Cyclic elastoplastic large displacement behavior of steel compression members. *Journal of Structural Engineering,* JSCE, Japan, Vol. 42A, pp. 135-145.

Mamaghani, I.H.P., Usami, T., and Mizuno, E. (1997). Hysteretic behavior of compact steel box beam- columns. *Journal of Structural Engineering*, JSCE, Japan, Vol. 43A, pp. 187-194.

Mamaghani, I.H.P., Shen, C., Mizuno, E., and Usami, T. (1995). Cyclic behavior of structural steels. I: experiments. *Journal of Engineering Mechanics*, ASCE, USA, Vol.121, No.11, pp. 1158-1164.

Shen, C., Mamaghani, I.H.P., Mizuno, E.,and Usami, T. (1995). Cyclic behavior of structural steels. II: theory. *Journal of Engineering Mechanics*, ASCE, USA, Vol.121, No.11, pp. 1165-1172.

Zienkiewicz, O.C. (1977). *The finite element method*. 3rd Ed., McGraw-Hill, New York.

Iraj H.P. Mamaghani is an Associate Professor of Civil Engineering at University of North Dakota. He received his B.Sc. in Civil Engineering from Istanbul Technical University with Honors in 1989. He continued his Master and PhD studies at University of Nagoya, Japan, where he obtained his Master and Doctor of Engineering degrees in Civil Engineering. Dr. Mamaghani has published several papers in professional journals and in conference proceedings. Dr. Mamaghani works in the area of civil engineering, with emphasis on structural mechanics and structural engineering. He focuses on cyclic elastoplastic material modeling, structural stability, seismic design, advanced finite element analysis and ductility evaluation of steel and composite (concrete-filled steel tubular) structures.